九州工業大学学術機関リポジトリ

Kyutacar

Kyushu Institute of Technology Academic Repository

Scale effect of slip boundary condition at solid liquid interface

SCIENTIFIC REPORTS

Scale effect of slip boundary condition at solid–liquid interface

Gyoko Nagayama, Takenori Matsumoto, Kohei Fukushima & Takaharu Tsuruta

Rapid advances in microelectromechanical systems have stimulated the development of compact devices, which require effective cooling technologies (e.g., microchannel cooling). However, the inconsistencies between experimental and classical theoretical predictions for the liquid flow in microchannel remain unclarified. Given the larger surface/volume ratio of microchannel, the surface effects increase as channel scale decreases. Here we show the scale effect of the boundary condition at the solid–liquid interface on single-phase convective heat transfer characteristics in microchannels. We demonstrate that the deviation from classical theory with a reduction in hydraulic diameters is due to the breakdown of the continuum solid–liquid boundary condition. The forced convective heat transfer characteristics of single-phase laminar flow in a parallel-plate microchannel are investigated. Using the theoretical Poiseuille and Nusselt numbers derived under the slip boundary condition at the solid–liquid interface, we estimate the slip length and thermal slip length at the interface.

Heat and mass transfer in microchannels has been extensively investigated over the past several decades. Continuum theory is applicable to single-phase liquid flow in microchannels, which implies that the equations developed for macroscale applications, such as the Navier–Stokes equation and convective heat transport equations, will be applicable to even small channels[1–5]. In a fully developed laminar channel flow, the classical theoretical solutions for the Nusselt number (hereafter, N_u; $N_u = \alpha D_h / \lambda_l$, where α is the convective heat transfer coefficient, D_h is the hydraulic diameter of a channel, and λ is the thermal conductivity) and Poiseuille number (hereafter, P_o; $P_o = f R_e$, where f is the Fanning friction factor and R_e is the Reynolds number) are constants and are independent of the Reynolds number. Because αD_h is nearly a constant, the forced convection heat transfer coefficients in fully developed laminar channel flows are expected to increase with a decrease in the microchannel size.

Table 1 lists the typical N_u and P_o values for a fully developed laminar flow in various channels[6], where N_{uT} is the N_u at a uniform surface temperature, and N_{uq} is the N_u at a uniform heat flux. The ratio of N_{uq} to N_{uT} is larger than 1. The N_{uT} listed in the table is the lower limit of N_u because the axial conduction effect is absent when the surface temperature is uniform. In other words, N_u cannot be less than N_{uT} in a thermally developing flow or in a flow under uniform surface heat flux accompanied by axial conduction. However, the experimental N_u for the forced convection of a single-phase liquid flow in Si microchannels differs significantly from that predicted using continuum theory[7–20]. These significant differences have been mainly attributed to experimental errors pertaining to the effects of axial conduction[16–18] and roughness[19–20]. However, because most studies report similar behaviours (i.e., N_u in microchannels decreases with decreasing R_e), the discrepancies between the theoretical and experimental results cannot be completely attributed to experimental errors. Davis and Gill[21], who were among the first to examine the axial conduction effect in laminar flow between parallel plates, concluded that the axial conduction effect reduced N_u. Other researchers[12,16–18] reported that the difference between experimental and theoretical N_u increased with decreasing R_e in microchannels could be attributed to the effects of axial heat conduction. On the other hand, the analytical results reported by Maranzana et al.[17] and Lin et al.[18] for the effects of axial heat conduction on single-phase microchannel flows yielded a much lower value of N_u than the theoretical results, which is in contrast to the conventional predictions of $N_{uq} > N_{uT}$ as the axial conduction increases. Thus, whether N_u can be less than N_{uT}, which is the lower limit of N_u without the axial conduction effect under uniform surface temperature, remains unresolved.

Here we focus on the scale effect on single-phase convective heat transfer in microchannels. We demonstrate that the deviation of N_u from that in classical theory with a reduction in the hydraulic diameters of the microchannels is due to solid–liquid interfacial resistance, which can be expressed in terms of the slip length

Department of Mechanical Engineering, Kyushu Institute of Technology, Tobata, Kitakyushu, Fukuoka 804-8550, Japan. Correspondence and requests for materials should be addressed to G.N. (email: nagayama@mech.kyutech.ac.jp)

Channels	N_{uq}	N_{uT}	N_{uq}/N_{uT}	P_o
Parallel plates				
1-side heated/1-side insulated	5.38	4.86	1.11	24
2-side heated	8.24	7.54	1.09	24
Square	3.63	2.98	1.22	56
Circular	4.36	3.66	1.19	64

Table 1. Nusselt and Poiseuille numbers for a fully developed laminar flow in various channels[6].
N_{uq} = Nusselt number at uniform surface temperature; N_{uT} = Nusselt number at uniform heat flux; P_o = Poiseuille number.
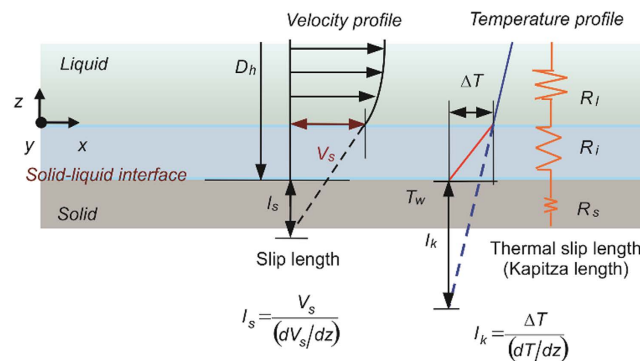
Figure 1. Slip boundary condition at the solid–liquid interface: slip length and thermal slip length.

and the thermal slip length (i.e., the Kapitza length). In addition, the convective heat transfer characteristics of single-phase laminar flow in parallel-plate microchannels are investigated experimentally. Finally, using the theoretical P_o and N_u numbers derived under the slip boundary condition at the solid–liquid interface, we estimate the slip length and thermal slip length at the interface.

Models and Methods

Slip boundary condition at solid–liquid interface. The boundary condition at the solid–liquid interface is a factor that strongly influences the thermohydraulic characteristics of single-phase liquid flow in microchannels. The continuum boundary condition (i.e., no-slip boundary condition) may fail because of the molecular interactions at the solid–liquid interface, and the slip boundary condition may be significant in nanochannel flow[22–26]. According to the Navier's model, the slip velocity at solid–liquid boundaries is linearly proportional to the velocity gradient at the surface:

$$V_s = l_s \cdot (dV/dz), \tag{1}$$

where l_s is the hydrodynamic slip length. Slip length l_s can be obtained by extrapolating the velocity profile from the position at the solid–liquid interface in the fluid to the position at which the velocity becomes zero, as shown in Fig. 1. Analogously, the slip thermal boundary condition can be determined using the "thermal slip length", that is, the position at which the temperature difference between the liquid and solid is zero. The physical meaning of thermal slip length, also known as the Kapitza length l_k, is the thickness of the thermal resistance at the solid–liquid interface:

$$l_k = \Delta T/(dT/dz) = R_i \lambda_l. \tag{2}$$

Here, ΔT is the temperature jump of the first layer of liquid located at the interface, dT/dz is the temperature gradient of the liquid, R_i is the thermal resistance at the solid–liquid interface, and λ_l is the thermal conductivity of the liquid.

Forced convection for fully developed laminar flow under slip boundary condition. Consider a parallel-plate Poiseuille flow subjected to constant heat flux at one channel wall in the steady state (Fig. 2). If the spacing between the parallel plates $2h$ is small relative to the size of the parallel plates, the hydraulic diameter is $D_h = 4h$. Assuming that the flow is incompressible and that all of the thermophysical properties are constant, the velocity profile of a hydrodynamic fully developed laminar flow under the slip boundary condition at both channel walls can be derived as follows:

$$U(z) = -\frac{h^2}{2\mu}\frac{dP}{dx}\left\{\left[1 - \left(\frac{z}{h}\right)^2 + 2\frac{l_s}{h}\right]\right\}, \tag{3}$$
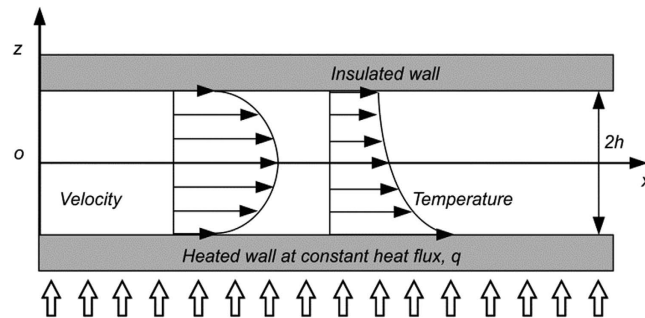
Figure 2. Parallel-plate Poiseuille flow under slip boundary condition.
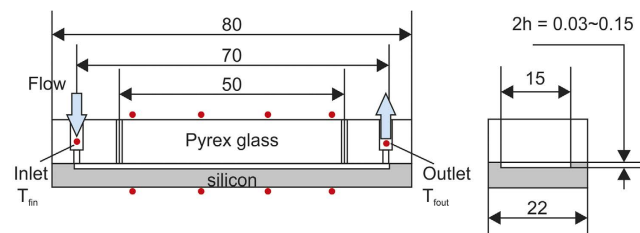
Figure 3. Si microchannel test section.

where μ is the viscosity and dP/dx is the pressure drop. For a fully developed laminar flow, P_o is

$$P_o = fR_e = \frac{24(l_s^* + 1)}{4l_s^* + 1},$$

(4)

where $l_s^* = l_s/(2h)$ and f is the fanning friction factor. For $l_s = 0$ or $l_s \gg 2h$, Eqs (3) and (4) agree with the theoretical predictions under the continuum assumption and P_o is a constant ($=24$). N_u can be obtained as

$$N_u = \frac{4(4/3 + 8l_s^*)^2}{1.32 + 4l_s^*(3.73 + 32l_s^*/3) + 2l_k^*(4/3 + 8l_s^*)^2},$$

(5)

where $l_k^* = l_k/(2h)$. For $l_s = 0$ or $l_s \gg 2h$ and $l_k = 0$ or $l_k \gg 2h$, Eq. (5) agrees with the theoretical prediction under the continuum assumption, and N_u is a constant ($=5.38$).

When the critical dimension of the flow decreases to a size comparable with that of the liquid molecule, l_s and l_k can no longer be ignored, and the slip boundary condition begins to strongly influence the momentum transfer and heat transfer characteristics in the microchannels. In particular, the solid–liquid interfacial resistance is dependent on the molecular interaction, that is, the contact condition between the liquid and the channel wall. Therefore, for a macroscopic smooth wall or a nanostructured wall, the scale effect of the interfacial resistance due to surface roughness and surface wettability becomes increasingly apparent.
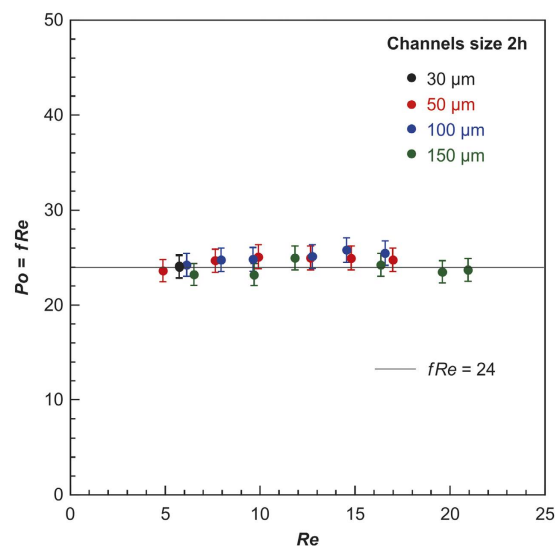
Experiment

Si-based microchannel test section. Si-based microchannels (70 mm (length) × 15 mm (width); 4 channel depths: 30, 50, 100, 150 μm) were prepared through KOH wet-etching of p-type Si wafers in the <100> orientation. The etched microchannels had a rectangular cross-section, as shown in Fig. 3. A Pyrex glass cover was anodically bonded to the Si wafer substrate at 350 °C and 2.0 kV to seal the microchannel, after which the parallel-plate microchannel test section was fabricated. Given that the depths of the microchannels were small relative to their widths and lengths, the channel hydraulic diameter D_h was nearly twice the channel depth (i.e., $D_h = 60, 100, 200$, and 300 for the four aforementioned channel depths).

To measure the pressure drop, two holes spaced 50 mm apart were fabricated in the cover glass in order to connect to a differential pressure sensor. On the backside of the microchannel, an aluminium thin film heater was sputtered, rendering the Si-based microchannel surface a heated wall subject to constant heat flux. The initial water contact angle at the fresh and clean Si surface was 58° ± 3°, but it decreased to 36° ± 3° because of the oxidation of the thin SiO_2 film. This surface served as the microchannel surface which the slip boundary condition was applied. The test section was finally assembled, and the bottom surface of the microchannel substrate and the top cover glass surface were well insulated to reduce heat loss from the test section.

Experimental apparatus. The experimental apparatus is shown in Fig. 4, which is consisted of a tank, a pump, valves, the test section of the Si-based microchannel, and a balance. Pure water (Kishida Chemical;
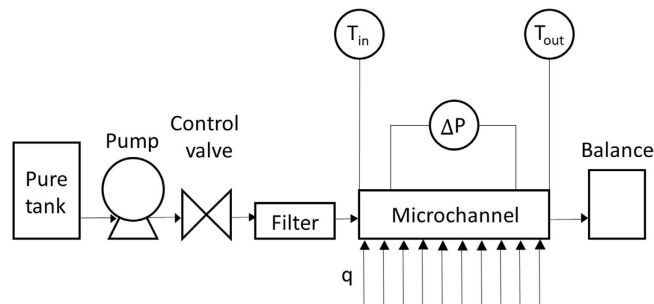
Figure 4. Schematic of experimental apparatus.

Figure 5. Experimental Poiseuille numbers P_o vs. Reynolds number R_e in microchannels.

electrical resistivity $= 18\,M\Omega cm$) was used as the working fluid. The fluid temperatures were measured using a T-type thermocouple (diameter $= 0.2\,mm$) at both the inlet and outlet. The wall temperatures were measured using eight T-type thermocouples. All of the pressure and temperature data were collected at $25\,°C$ and $40\,RH\%$ by using a data logger and then transmitted to a computer.

Results and Discussions

Experimental Poiseuille Number. The friction factor f is obtained from the pressure drop ΔP, the distance over which the pressure is measured L in the fully developed flow region, the fluid density ρ, and the mean velocity of the working fluid U, as shown in Eq. (6).

$$f = \Delta P D_h/(2\rho U^2 L) \tag{6}$$

Then, the Po number can be obtained as follows.

$$P_o = f R_e = \frac{2wh^3 \triangle T}{\nu L \dot{m}}, \tag{7}$$

where the microchannel width w is $15\,mm$, $\dot{m}$ is the mass flow rate, and ν is the dynamic viscosity of the working fluid.

Figure 5 shows the experimental results for the Poiseuille number in the microchannels with hydraulic diameters D_h of $60\,\mu m$, $100\,\mu m$, $200\,\mu m$, and $300\,\mu m$, respectively. The results obtained for the Poiseuille number (from more than 3 different independent experiments) agree well with the theoretical values, based on the continuum boundary condition. This could be explained by the surface being covered in a thin, hydrophilic SiO_2 film and the slip velocity being negligible in the studied cases.

Experimental Nusselt number. The heat flux supplied to the heater includes the heat flux through forced convection for heat exchange between the Si microchannel surface and the working fluid, as well as the heat flux through axial conduction inside the Si microchannel substrate. To avoid the axial conduction effect, the method whereby heat flux is supplied to the heater has not been used in the present study. The heat flux exchanged at the microchannel surface, q is obtained from the temperature difference at the fully developed flow region,
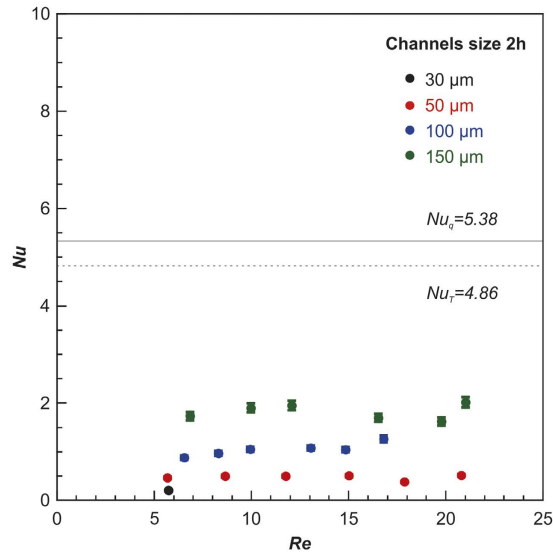
Figure 6. Experimental Nusselt numbers N_u vs. Reynolds number R_e in microchannels.

$$q = \dot{m}C_p(T_{f1} - T_{f2})/\mathrm{A} \tag{8}$$

where C_p is the specific heat of the liquid and A is the equivalent surface area for heat transfer. The mean heat transfer coefficient and the Nusselt number are obtained as follows.

$$\alpha = \frac{q}{\Delta \overline{(T_w - T_f)}} = \frac{\dot{m}C_p(T_{f1} - T_{f2})}{\Delta \overline{(T_w - T_f)} \cdot A} \tag{9}$$

$$N_u = \frac{\alpha D_h}{\lambda_l} \tag{10}$$

where $\Delta \overline{(T_w - T_f)}$ is the mean temperature difference between the channel wall and the working fluid.

Figure 6 shows the experimentally obtained Nusselt numbers for the microchannels with hydraulic diameter D_h of 60 μm, 100 μm, 200 μm, and 300 μm, respectively. The experimental Nu numbers are much lower than the theoretical values of both Nu_q (constant heat flux) and Nu_T (constant surface temperature) based on the continuum boundary condition. The deviations between the experimental Nu and theoretical Nu increase as the hydraulic diameter of the microchannel decreases.

Scale effects of interfacial resistances. The interfacial resistance (i.e., l_s and l_k) can be estimated from the difference between continuum theory and the experimental results. Using Eq. (4) and the experimental mean P_o ($=fR_e$), l_s can be estimated as follows:

$$l_s{}^* = l_s/2h = (24 - fR_e)/(4fR_e - 24). \tag{11}$$

Similarly, l_k can be estimated using the experimental mean N_u and Eq. (5):

$$l_k{}^* = \frac{l_k}{2h} = \frac{2}{N_u} - \frac{1.32 + 4l_s{}^*(3.73 + 32l_s{}^*/3)}{2(4/3 + 8l_s{}^*)^2}. \tag{12}$$

Next, the forced convective heat transfer characteristics of the single-phase laminar flow in a parallel-plate microchannel are investigated experimentally. Figures 7 and 8 illustrate the experimental results and theoretical predictions, respectively, to clarify the scale effect of the hydraulic diameter on forced convection in microchannels. The theoretical P_o is $(fR_e)_{th} = 24$, 64, and 57 for the parallel-plate channel, circular tube of refs 27 and 28, and the rectangular channel of Ref. 27, respectively (Fig. 3)[27,28]. The slip length of the water and silicon oxide interface in the present study can be assumed to be 0 because the experimental results agree well with the theoretical predictions. However, the experimental results obtained by Judy *et al.*[27] in rectangular channels decrease with decreasing hydraulic diameter, which agrees fairly well with the theoretical prediction of $l_s = 1$ μm, for which the error is less than 2%.

In contrast to the foregoing results, the experimental N_u in Fig. 8 is significantly lower than the theoretical N_u under the no-slip boundary condition. The experimental N_u decreases with decreasing hydraulic diameter, whereas the discrepancy decreases with increasing hydraulic diameter, which is consistent with the trends reported in the literature[8,9]. The experimental N_u obtained in this study agrees well with the theoretical prediction
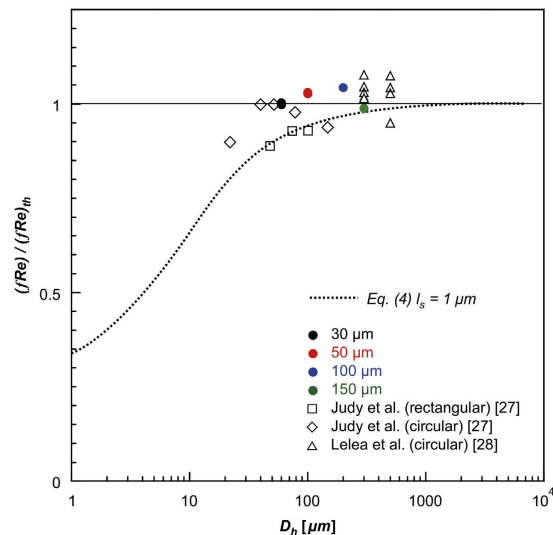
Figure 7. Scale effect of slip length on hydrodynamic resistance in microchannels.
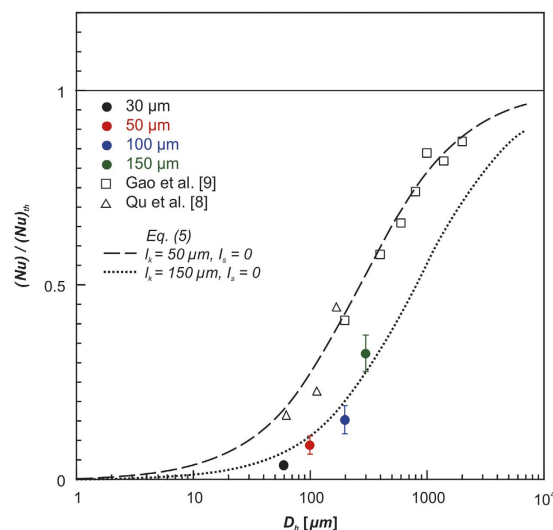
Figure 8. Scale effect of thermal slip length on convective heat transfer in microchannels.

of $l_s = 0\,\mu m$ and $l_k = 150\,\mu m$, while those reported by Qu et al.[8] and Gao et al.[9] agree well with the theoretical prediction of $l_s = 0\,\mu m$ and $l_k = 50\,\mu m$. In other words, the slip length and thermal slip length can no longer be ignored when these lengths are comparable with the hydraulic diameter. Therefore, we conclude that the scale effect explains the difference between the predictions of continuum theory and the experimental results.

Surface roughness[19,20] exerts significant effects on forced convection heat transfer in microchannels. Moreover, surface wettability strongly affects convective heat transfer in microchannels[29], and effective slip and friction reduction in nanograted superhydrophobic microchannels have been reported[30]. The effects of roughness and wettability, which are types of interfacial resistance, can be expressed using slip length and thermal slip length when the continuum boundary condition fails. Additional theoretical, molecular dynamics simulation[26,31–34], and experimental studies[35] on interfacial resistance are warranted to further clarify the mechanism.

Summary

We studied the scale effect of the boundary condition at the solid–liquid interface on the single-phase convective heat transfer characteristics in microchannel or nanochannel flow. We have shown that the increasing inaccuracy of the predictions of classical theory with a decrease in the hydraulic diameter is due to the breakdown of the continuum solid–liquid boundary condition in microchannels. In other words, the solid–liquid interfacial resistance, which can be expressed as the slip length and thermal slip length, cannot be ignored when these lengths are comparable with the hydraulic diameter. Using the theoretical P_o and N_u derived under the slip boundary condition at the solid–liquid interface, we can estimate the slip length and thermal slip length at the solid–liquid interface.

References

1. Kandlikar, S. G. History, advances, and challenges in liquid flow and flow boiling heat transfer in microchannels: a critical review. *ASME J. Heat Transfer* **134,** 034001-1–0344001-15 (2012).
2. Kandlikar, S. G. *et al*. Heat transfer in microchannels—2012 status and research needs. *ASME J. Heat Transfer* **135,** 091001-1–091001-18 (2013).
3. Wang, G., Liang, H. & Cheng, P. An experimental and numerical study of forced convection in a microchannel with negligible axial heat conduction. *Int. J. Heat Mass Transfer* **52,** 1070–1074 (2009).
4. Dixit, T. & Ghosh, I. Review of micro- and mini-channel heat sinks and heat exchangers for single phase fluids. *Renewable Sustainable Energy Rev*. **41,** 1298–1311 (2015).
5. Morini, G. L. Single-phase convective heat transfer in microchannels: a review of experimental results. *Int. J. Thermal Sciences* **43,** 631–651 (2004).
6. Nishikawa, K. & Fujita, Y. *Heat Transfer* 142 (Rikogakusha, Tokyo, 1982).
7. Peng, X. F. & Peterson, G. P. Convective heat transfer and flow friction for water flow in microchannel structures. *Int. J. Heat Mass Transfer* **39,** 2599–2608 (1996).
8. Qu, W., Mala, G. M. & Li, D. Heat transfer for water flow in trapezoidal silicon microchannels. *Int. J. Heat Mass Transfer* **43,** 3925–3936 (2000).
9. Gao, P., Person, S. L. & Favre-Marinet, M. Scale effects on hydrodynamics and heat transfer in two-dimensional mini and microchannels. *Int. J. Thermal Sciences* **41,** 1017–1027 (2002).
10. Wu, H. Y. & Cheng, P. An experimental study of convective heat transfer in silicon microchannels with different surface conditions. *Int. J. Heat Mass Transfer* **46,** 2547–2556 (2003).
11. Guo, Z. Y. & Li, Z. X. Size effect on microscale single-phase flow and heat transfer. *Int. J. Heat Mass Transfer* **46,** 149–159 (2003).
12. Hetsroni, G., Mosyak, A., Pogrebnyak, E. & Yarin, L. P. Heat transfer in micro-channels: comparison of experiments with theory and numerical results. *Int. J. Heat Mass Transfer* **48,** 5580–5601 (2005).
13. Shen, S., Xu, J. L., Zhou, J. J. & Chen, Y. Flow and heat transfer in microchannels with rough wall surface. *Energy Conversion Management* **46,** 1311–1325 (2006).
14. Rosa, P., Karayiannis, T. G. & Collins, M. W. Single-phase heat transfer in microchannels: the importance of scaling effects. *Appl. Therm. Eng*. **29,** 3447–3468 (2009).
15. Nagayama, G., Sibuya, S., Kawagoe, M. & Tsuruta, T. Heat transfer enhancement at nanostructured surface in parallel-plate microchannel. *Challenges Power Eng. Env.* 999–1006 (2007).
16. Tiselj, I. *et al*. Effect of axial conduction on the heat transfer in micro-channels. *Int. J. Heat Mass Transfer* **47,** 2551–2565 (2004).
17. Maranzana, G., Perry, I. & Maillet, D. Mini- and micro-channels: influence of axial conduction in the walls. *Int. J. Heat Mass Transfer* **47,** 3993–4004 (2004).
18. Lin, T. Y. & Kandlikar, S. G. A theoretical model for axial heat conduction effects during single-phase flow in microchannels. *J. Heat Transfer* **134,** 020902-1–020902-6 (2012).
19. Koo, J. & Kleinstreuer, C. Analysis of surface roughness effects on heat transfer in micro-conduits. *Int. J. Heat Mass Transfer* **48,** 2625–2634 (2005).
20. Gamrat, G., Favre-Marinet, M. & Person, S. L. Modelling of roughness effects on heat transfer in thermally fully-developed laminar flows through microchannels. *Int. J. Thermal Sciences* **48,** 2203–2214 (2009).
21. Davis, E. J. & Gill, W. N. The effects of axial conduction in the wall on heat transfer with laminar flow. *Int. J. Heat Mass Transfer* **13,** 459–470 (1970).
22. Thompson, P. A. & Troian, S. M. A general boundary condition for liquid flow at solid surfaces. *Nature* **389,** 360–362 (1997).
23. Nagayama, G. Boundary conditions and microscale heat transfer at solid-liquid interface. *J. Heat Transfer Soc. Jpn*. **50,** 29–36 (2011).
24. Nagayama, G. & Cheng, P. Effects of interface wettability on microscale flow by molecular dynamics simulation. *Int. J. Heat Mass Transfer* **47,** 501–513 (2004).
25. Nagayama, G., Tsuruta, T. & Cheng, P. Molecular dynamics simulation on bubble formation in a nanochannel. *Int. J. Heat Mass Transfer* **49,** 4437–4443 (2006).
26. Nagayama, G., Kawagoe, M., Tokunaga, A. & Tsuruta, T. On the evaporation rate of ultra-thin liquid film at the nanostructured surface: a molecular dynamics study. *Int. J. Thermal Sciences* **49,** 59–66 (2010).
27. Judy, J., Maynes, D. & Webb, B. W. Characterization of frictional pressure drop for liquid flows through microchannels. *Int. J. Heat Mass Transfer* **45,** 3477–3489 (2002).
28. Lelea, D., Nishio, S. & Takano, K. The experimental research on microtube heat transfer and fluid flow of distilled water. *Int. J. Heat Mass Transfer* **47,** 2817–2830 (2004).
29. Rosengarten, G., Cooper-White, J. & Metcalfe, G. Experimental and analytical study of the effect of contact angle on liquid convective heat transfer in microchannels. *Int. J. Heat Mass Transfer* **49,** 4161–4170 (2006).
30. Choi, C. H. *et al*. Effective slip and friction reduction in nanograted superhydrophobic microchannels. *Physics Fluids* **18,** 087105 (2006).
31. Torii, D., Ohara, T. & Ishida, K. Molecular-scale mechanism of thermal resistance at the solid-liquid interfaces: influence of interaction parameters between solid and liquid molecules. *J. Heat Transfer* **132,** 012402-1–012402-9 (2010).
32. Wang, C. *et al*. Friction reduction at a superhydrophilic surface: role of ordered water. *J. Phys. Chem. C* **119,** 11679–11684 (2015).
33. Falk, K. *et al*. Molecular origin of fast water transport in carbon nanotube membranes: superlubricity versus curvature dependent friction. *Nano Lett.* **10,** 4067–4073 (2010).
34. Chen, J., Walther, J. H. & Koumoutsakos, P. Strain engineering of Kapitza resistance in few-layer graphene. *Nano Lett.* **14,** 819–825 (2014).
35. Hopkins, P. E. *et al*. Measuring the thermal conductivity of porous, transparent SiO2 films with time domain thermoreflectance. *J. Heat Transfer* **133,** 061601-1–061601-8 (2011).

Acknowledgements

Author Contributions

G.N. performed the structural determination and theoretical analyses, conceived the experimental design, and wrote the paper. T.M. and K.F. conducted the experiments and theoretical analyses under the supervision of G.N. All of the authors have discussed the results and have commented on the manuscript.

Additional Information

Competing financial interests: The authors declare no competing financial interests.

How to cite this article: Nagayama, G. *et al.* Scale effect of slip boundary condition at solid–liquid interface. *Sci. Rep.* **7**, 43125; doi: 10.1038/srep43125 (2017).

Publisher's note: Springer Nature remains neutral with regard to jurisdictional claims in published maps and institutional affiliations.